Original Article

Investigating the Effect of Selenium Nanoparticles on Mineral Trioxide Aggregates as a Promising Novel Dental Material

Njwan F. Shehab[1], Nadia H. Hasan[1], Hana K. Ismail[2]

[1]Department of Conservative Dentistry, College of Dentistry, [2]Department of Pathology and Poultry Disease, College of Veterinary Medicine, University of Mosul, Mosul, Iraq

ABSTRACT

Aim: To enhance mineral trioxide aggregate high plasticity (MTA HP), a commonly used dental calcium silicate cement, by incorporating selenium nanoparticles (SeNPs) known for their antioxidant and anti-inflammatory properties. The objectives included investigating the impact of SeNPs on the setting time and chemical properties of MTA HP. **Materials and Methods:** We performed a comprehensive study to formulate and profile SeNPs integrated into MTA HP. Diverse concentrations of SeNPs were introduced into MTA HP, and the commencement and culmination of the setting process were gauged employing a Gillmore needle cabinet. The chemical composition was validated using Fourier transform infrared spectroscopy with attenuated total reflectance and X-ray diffraction analysis. **Results:** The incorporation of SeNPs led to remarkable improvements. Notably, SeNPs positively affected the setting time of MTA HP, with faster setting times corresponding to higher SeNPs concentrations. Chemical analyses confirmed the successful integration of SeNPs with MTA HP. These enhancements make the material may be suitable for dental applications, especially due to its accelerated setting time. **Conclusions:** MTA HP incorporated with SeNPs represents a significant advancement in dental materials. Its faster setting time, combined with the antioxidant and anti-inflammatory properties of selenium, provides dental professionals with an efficient and time-saving option for complex treatments. This novel nanomaterial holds promise for improving dental procedures and patient outcomes.

KEYWORDS: *Fourier transform infrared spectroscopy with attenuated total reflectance, mineral trioxide aggregate repair high plasticity, selenium nanoparticles, setting time, X-ray diffraction*

Received : 27-Sep-2023
Revised : 06-Nov-2023
Accepted : 01-Dec-2023
Published : 27-Feb-2024

INTRODUCTION

The field of dentistry constantly seeks innovative materials that can improve treatment outcomes and patient comfort. Mineral trioxide aggregate (MTA) has been widely used in endodontic procedures. However, MTA has limitations, such as low plasticity and long setting time. To overcome these drawbacks, researchers have explored the incorporation of nanoparticles into MTA to develop a novel material with enhanced properties. Due to their unique properties, selenium nanoparticles (SeNPs) have gained attention in various fields, including dentistry. SeNPs exhibits excellent biocompatibility and antioxidant activity, which

Access this article online

Quick Response Code:

Website: https://journals.lww.com/jpcd

DOI: 10.4103/jispcd.jispcd_148_23

Address for correspondence: Dr. Njwan Fadhel Shehab, Department of Conservative Dentistry, College of Dentistry, University of Mosul, Mosul 41001, Iraq.
E-mail: njwandent@uomosul.edu.iq

How to cite this article: Shehab NF, Hasan NH, Ismail HK. Investigating the effect of selenium nanoparticles on mineral trioxide aggregates as a promising novel dental material. J Int Soc Prevent Communit Dent 2024;14:16-27.

can contribute to tissue healing and regeneration. Moreover, SeNPs have demonstrated antimicrobial effects against common oral pathogens, making them suitable candidates for dental applications.[1] The search results did not provide specific information about how SeNPs affect the properties of dental materials. However, some studies have investigated the potential benefits of incorporating SeNPs into dental materials, such as enhanced antibacterial and anti-inflammatory properties, SeNPs have been reported to have antibacterial and anti-inflammatory properties.[2] Incorporating SeNPs into dental materials could enhance their ability to fight against bacterial infections and inflammation. Improved physicomechanical properties: SeNPs have been studied for their potential to improve the physicomechanical properties of dental materials. For example, selenium is reported to be involved in synthetic hydroxyapatite through phosphate change with selenite. The ionic radius of Se^{+4} is higher than P^{+5} (phosphate) value. For this reason, the fabric parameter increases after it is settled in synthetic hydroxyapatites. Incorporating SeNPs into dental materials could potentially improve their strength, durability, and other mechanical properties.[3,4] Potential use as delivery carriers for chemotherapy: it has been studied as delivery carriers to encapsulate drugs or chemotherapy. Incorporating SeNPs into dental materials could potentially provide a new approach to drug delivery in dental applications.[3] It is important to carefully evaluate the effects of SeNPs on dental tissues before incorporating them into dental materials. The optimal concentration of SeNPs for dental applications is not well established. A study hypothesized that SeNPs at different concentrations can exert different effects on the MTA HP repair material. Potential challenges associated with incorporating SeNPs into dental materials include determining the optimal concentration, biocompatibility,[5] and cost. Further research is needed to address these challenges and determine the potential benefits of incorporating SeNPs into dental materials. In summary, selenium nano is safe and has the intrinsic property of catalyzing short-lived free radicals to destroy nearby bacterial cells. MTA HP has desirable features, such as bioactivity, hydrophilicity, sealing ability, and low solubility. The incorporation of SeNPs into MTA HP could potentially lead to the development of a viable material for dental applications. However, the specific analysis of Fourier transform infrared spectroscopy with attenuated total reflectance (ATR-FTIR) spectra of hydrated MTA HP with SeNPs in dental applications is not well established. Research is needed to determine the potential benefits of incorporating SeNPs into MTA HP. Hence, this study aims to assess how incorporating SeNPs impacts the setting time of MTA HP as well as investigate any potential chemical interactions between SeNPs and MTA HP that could be relevant to the development of pulp capping materials. Therefore material's properties will be thoroughly investigated using various characterization techniques, including ATR-FTIR, X-ray diffraction (XRD), and setting time assessments. The characterization aims to comprehensively understand the effect of SeNPs on the MTA HP. Such information is crucial for evaluating the material's potential as a promising dental material and guiding its further optimization for specific clinical applications. The hypothesis posited in this study is that SeNPs do not impact the setting time of MTA HP.

Materials and Methods

Sample preparation

The sample preparation involved mixing various amounts of green-synthesized SeNPs powder (99.9% purity, spherical particles; Nano Research Elements, Kurukshetra, India) with the powder of the tested pulp capping agent. Five groups with different concentrations of nanoparticles (group I [control]: 0% w/w SeNPs, group II: 0.5% w/w SeNPs, group III: 1% w/w SeNPs, group IV: 1.5% w/w SeNPs, and group V: 2% w/w SeNPs) were tested to measure the initial and final setting time. The commercially available MTA Repair HP (Angelus, Londrina, Brazil) was tested in the present study. The MTA HP was prepared by mixing the powder with liquid manually in a glass plate using a metallic spatula for 40 s to obtain a homogeneous consistency, as recommended by the manufacturer.

Setting time

The setting time is the duration from mixing the material until no indentation or mark can be made on the specimen surface using a Gillmore needle cabinet. This is determined by monitoring the penetration depth of the needle. As the material sets and hardens, the penetration depth decreases. The setting time is considered reached when the needle no longer makes any indentations. The determination of the initial and final setting times for all samples followed the guidelines outlined in the American Society for Testing and Materials specification no. C266-21. However, the samples were prepared by the American National Standard/American Dental Association specification no. 96 for Dental Water-Based Cements (2020).

The initial setting time was determined by subjecting the sample to a load of (113.4 ± 0.5) g using a needle with a flat tip diameter of (2.12 ± 0.05) mm. The final set time was determined using a cylindrical indenter

with a flat tip diameter of (1.06 ± 0.05) mm and a weight of (453.6 ± 0.5) g. Before preparing the samples, the Gillmore cabinet was conditioned in an incubator at (37 ± 1)°C and 95% relative humidity for at least 1 h.

Five stainless-steel molds with an inner diameter of 10 mm and a height of 5 mm were utilized to create the specimens under examination. Each mold was positioned on a glass slide and filled with the tested cement, prepared according to the manufacturer's guidelines. Following mixing period, the filled mold, along with its glass slide, was placed on the metal block of the Gillmore cabinet. An indenter known as the Gillmore needle, weighing (113.4 ± 0.5) g and featuring a flat end with a diameter of (2.12 ± 0.05) mm, was then carefully lowered vertically onto the material's surface and left undisturbed for 5 s. Any indentation observed on the surface indicated that the material had not yet set. The needle tip was cleaned, and this procedure was repeated until no fresh marks or complete circular indentations were discernible on the cement surface, as determined through visual inspection. To determine the final setting time, a different Gillmore needle weighing (453.6 ± 0.5) g, possessing a tip diameter of (1.06 ± 0.05) mm, was employed using the same technique. The initial and final setting times were recorded when the Gillmore needles were no longer capable of producing visible marks on the surface.

Analysis using ATR-FTIR

The Alpha II Bruker ATR-FTIR spectrometer (ATR-FTIR, Alpha II Bruker, Germany) was utilized to conduct infrared spectroscopic measurements. Spectra were acquired in the transmission mode using the OPUS software, Bruker, Germany (version 8.5) provided by the spectrometer manufacturer, with a resolution of 4 cm^{-1} and 24 scans. The measurement spanned the range of 400–4000 cm^{-1}.

The FTIR spectra of SeNPs powder and the hydrated sample before and after incorporation of SeNPs were obtained by crushing them using a pestle and mortar. The resulting crushed material was carefully positioned in a designated hole on the diamond window of the device. Subsequently, the holder's head was manually adjusted to establish contact with the material. The scanning process was initiated, and data were collected using the OPUS software (version 8.5), as documented by Mahmoud *et al*. in 2022.[6]

X-ray analysis

The samples underwent XRD analysis using a Phillips X'pert PANanalytical X-ray diffractometer from Holland. The XRD analysis utilized a radiation source with Cu $K\alpha$ wavelength (λ = 1.54060 Å). The diffractometer was operated at 40.0 kV and 30 mA, and the analysis was performed in the range of diffraction angle (2θ) from 10° to 80°, with a step size of [2-Theta] 0.0500 and a scan step time of 1.0000 s. The exposure time was determined based on the specific requirements. Phase identification was achieved by employing search-match software that utilized the Joint Committee of Powder Diffraction Standard and International Center for Diffraction Data (JCPDS-ICDD) files. The prominent peaks from the data were used in the calculation to determine the crystalline size of green-synthesized SeNPs. This calculation was performed using Debye–Scherrer's equation as follows: $D = K\lambda/\beta\cos\theta$.

In this equation, D is the mean crystalline size of the particles, K is Scherrer's constant (0.9), λ is the X-ray wavelength of $K\alpha$ (0.15406 nm), β is the peak's full width at half maximum (FWHM) in radians, and θ is the Bragg angle in radians.[7]

To obtain the hydrated cement, specimens (3 mm diameter, 2 mm height) were prepared and allowed to set for 24 h at 37°C in a relative humidity of 95 ± 5%. The XRD investigation of hydrated MTA HP was performed both before and after the incorporation of SeNPs. Hydrated MTA HP with and without SeNPs was softly dispersed over the X-ray container. Using a dental spatula, the material was compacted on the X-ray holder. Extra cement was removed from the surface of the X-ray holder by a glass slide edge. The holder was examined visually to guarantee uniform and complete covering. When analyzing the phase of each material, the X-ray holder was mounted on a metal slide and then attached to an X-ray diffractometer.

Statistical analysis

Data distribution

[]The data were analyzed with SPSS 22 (Chicago, IL), and the data distribution was found to be normal using the Shapiro–Wilk's test. A one-way analysis of variance (ANOVA) was performed to determine significant differences among the groups for setting time. Tukey's test was used for multiple comparisons to determine which treatments were significantly different from each other.

Significance level

The significance level was set at $P \leq 0.05$.

Results

Setting time

The study aimed to evaluate the setting time of MTA HP incorporated with different concentrations of SeNPs. The setting time refers to the time required for the material to solidify or set. The experimental

design involved comparing the setting time between the experimental group (MTA HP with different concentrations of SeNPs) and the control group (MTA HP without SeNPs). In each group, five samples were taken for testing. To assess the statistical significance of the differences between groups, an ANOVA test was conducted. ANOVA is a statistical test used to compare means across multiple groups. The results of the ANOVA test are presented in Table 1.

The *P* value measures the probability of obtaining results as extreme as those observed, assuming there is no true difference between the groups. In both cases, $P \leq 0.05$, indicating a significant variation exists between the groups. These results suggest that the different concentrations of SeNPs incorporated into MTA HP have a significant effect on both the initial and final setting times.

Table 2 presents the means and standard deviations for the initial and final setting times of MTA HP with different concentrations of SeNPs. The table also includes the number of specimens (*N*) for each group. Tukey's tests were used for comparisons among the MTA and the various concentrations of SeNPs incorporated into it. For the initial setting time, incorporating 0.5% w/w SeNPs had no significant effect on the setting time, as indicated by the mean value of 14.9200 ± 0.37014 min (±SD). Other concentrations of SeNPs (1%, 1.5%, and 2% w/w) showed a decrease in the mean setting time compared to the control group. The mean values for the test groups were as follows: 13.3200 ± 0.40866 min for 1% w/w, 11.9200 ± 0.37014 min for 1.5% w/w, and 11.3200 ± 0.40866 min for 2% w/w. The test results indicate a significant difference ($P < 0.05$) between the 1% w/w concentration group and the other groups for the initial setting time. For the final setting time, incorporating different concentrations of SeNPs resulted in a shorter setting time compared to the control group. The mean values for the test groups were as follows: 83.1800 ± 0.61400 min for 0.5% w/w, 67.3200 ± 0.71903 min for 1% w/w, 66.1800 ± 0.61400 min for 1.5% w/w, and 38.3200 ± 0.81670 min for 2% w/w. The test results indicate a nonsignificant difference ($P > 0.05$) between the 1% w/w and 1.5% w/w concentration groups for the final setting time. In summary, incorporating 0.5% w/w SeNPs had no significant effect on the initial setting time, while other concentrations showed a decrease. The 1% w/w concentration group significantly differed from the other groups. For the final setting time, incorporating various concentrations of SeNPs resulted in a shorter setting time compared to the control group. There was no significant difference between the 1% w/w and 1.5% w/w concentration groups for the final setting time.

Table 1: ANOVA for initial and final setting time for MTA HP incorporated with different concentrations of SeNPs

		Sum of squares	df	Mean square	*F* value	*P* value*
Initial setting time	Between groups	58.800	4	14.700	115.748	0.000
	Within groups	2.540	20	0.127		
	Total	61.340	24			
Final setting time	Between groups	7190.990	4	1797.747	3450.571	0.000
	Within groups	10.420	20	0.521		
	Total	7201.410	24			

ANOVA = analysis of variance, MTA HP = mineral trioxide aggregate high plasticity, SeNPs = selenium nanoparticles, df = degree of freedom

*$P \leq 0.05$ mean significant variation exists

Table 2: Means and standard deviations for each initial and final setting time using Tukey's testing to compare MTA with and without varied SeNPs concentrations

SeNPs (%)		Mean ± SD		
		N	Initial setting (min)	Final setting (min)
Setting time (min)	0	5	15.1200 ± 0.16432^{C}	85.9800 ± 0.81670^{D}
	0.5	5	14.9200 ± 0.37014^{C}	83.1800 ± 0.61400^{C}
	1	5	13.3200 ± 0.40866^{B}	67.3200 ± 0.71903^{B}
	1.5	5	1.9200 ± 0.37014^{A}	66.1800 ± 0.61400^{B}
	2	5	1.3200 ± 0.40866^{A}	38.3200 ± 0.81670^{A}

The values in the table that are marked with different letters (A–D) indicate a significant difference among the groups at different concentrations of SeNPs for each initial and final setting time (%) at a significance level of $P \leq 0.05$

SeNPs = selenium nanoparticles, *N* = the number of specimens, SD = standard deviation

Fourier transform infrared spectroscopy with attenuated total reflectance

ATR-FTIR spectroscopy of MTA HP can provide valuable information about the composition, molecular structure, and chemical changes that occur during the setting process. This analysis can aid in optimizing the formulation and understanding the performance of MTA materials in dental applications. The identified peaks and functional groups are interpreted to gain insights into the composition and structure of MTA HP. This information can be used to assess the quality of the material, evaluate any chemical changes, and correlate them with the material's properties and clinical performance. The search results did not provide any specific information about how SeNPs affect the MTA HP in dental applications.

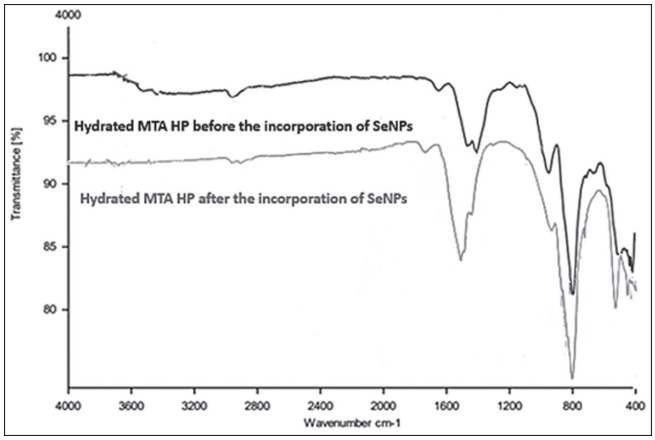

Figure 1: ATR-FTIR spectra of hydrated MTA HP before and after incorporation of SeNPs. ATR-FTIR = Fourier transform infrared spectroscopy with attenuated total reflectance, MTA HP = mineral trioxide aggregate high plasticity, SeNPs = selenium nanoparticles

The ATR-FTIR spectra [Figure 1 and Table 3] of hydrated MTA Repair HP (after setting) provide information related to functional groups. One of the significant findings is the presence of a sharp peak at ~422 cm^{-1}, which can be attributed to the lattice vibration (Ca–O) of hydrated tricalcium aluminate. This peak confirms the involvement of tricalcium aluminate in the chemical reaction. Additionally, the vibrational band at 860 cm^{-1} corresponds to the (Al–O) group, further supporting the presence of tricalcium aluminate. The ATR-FTIR analysis also revealed distinct vibrational bands corresponding to (Si–O) stretching at 798 cm^{-1} and (SiO_4) bending at 517 cm^{-1}, which are characteristic of (Ca_3SiO_5). Moreover, the results indicated the presence of a (SiO_4) bending group at 450 cm^{-1}, which is associated with (Ca_2SiO_4).

These findings demonstrate the involvement of calcium silicates in the chemical reaction. Furthermore, the broad band centered at 3440 cm^{-1} in the spectra can be attributed to the stretching vibrations of (O–H) adsorbed water molecules. This confirms the presence of water within the hydrated MTA HP sample. Additionally, the major vibrational bands at 3644 and 3523 cm^{-1} correspond to the (O–H) band of [$Ca(OH)_2$], indicating the formation of calcium hydroxide [$Ca(OH)_2$] as a result of the chemical reaction. Importantly, the shifting of the (Si–O) vibrational bands to higher wavenumbers at 925, 1100, 1152, and 1650 cm^{-1} is indicative of the dissolution of calcium silicate units to form calcium silicate hydrate (CSH). The vibration observed at 656 cm^{-1} can be attributed to (Si–O–Si) in (CSH) after hydration, further supporting this transformation. Furthermore, the presence of calcium carbonate ($CaCO_3$) was confirmed through ATR-FTIR analysis,

Table 3: The FTIR results for the hydrated MTA HP (set) materials

Material	Functional group and vibrational mode	Wavenumber (cm^{-1})	Experimental
$Ca(OH)_2$	O–H stretching groups (portlandite)	3644 and 3523	3644[15]
Adsorbed H_2O molecules	O-H stretching	3440	3400[9]
PVP	CH_2 stretching	2950	2950[20]
CSH	H–O–H stretching	1650	1640[15]
CSH	stretching	1100 and 1152	1138–1155[30]
CSH	Si–O stretching	925	925[31]
C_3A	Al–O stretching	860	860[9]
C_3S	Si–O stretching	798	810[21]
CSH	Si–O–Si bending	656	653[18]
C_3S	SiO_4 bending	517	515[32]
CSH	SiO_4 bending	495	494[31]
C_2S	SiO_4 bending	450	452[15]
Hydrated C_3A	Ca–O sharp bending	422	420[9]

FTIR = Fourier transform infrared, MTA HP = mineral trioxide aggregate high plasticity, PVP = Polyvinylpyrrolidone , CSH = calcium silicate hydrate, C_3S = tricalcium silicate, C_2S = dicalcium silicate, C_3A = tricalcium aluminate

with characteristic bands appearing at 1470 and 1413 cm^{-1}. The ATR-FTIR spectra and table of hydrated MTA HP provide comprehensive evidence the findings contribute to a better understanding of the hydration process and chemical transformations that take place within the MTA HP material after setting.

The incorporation of green-synthesized SeNPs into MTA HP has yielded significant advancements, making it a subject of great interest in the field. Our research provides valuable insights into the changes and enhancements observed in the material after this integration. This study presents compelling findings that shed light on the improved properties and potential applications of this innovative material. One of the key findings of this study is the analysis of the ATR-FTIR spectrum of the hydrated MTA HP incorporated with green-synthesized SeNPs. The spectrum revealed notable changes, including shifting of bands and the appearance of new bands, indicating the interaction between the MTA HP and SeNPs as shown in the ATR-FTIR spectrum [Figure 1 and Table 4]. Specifically, the shifting of bands at 1650 cm^{-1}, attributed to CSH, and the appearance of new bands at 1778 and 1659 cm^{-1} indicated the presence of calcium selenite, as indicated by the stretching vibration of (Se=O) and (SeO_3^{-2}) functional groups, respectively. Furthermore, the shifting of CSH bands at 1100, 1152, and 495 cm^{-1} to 1082 and 440 cm^{-1}, respectively, indicated the bending vibration of (SeO_3^{-2}) and (Se–O) groups. Another significant finding was the weak band at 837 cm^{-1}, which confirmed the presence of selenite (SeO_3^{-2}) groups. These results suggest that there is a reaction between (CSH) and SeNPs, leading to the replacement of selenium with silica within the structure of (CSH). The resulting compound is identified as calcium selenite ($Ca_2(SeO_3)(Se_2O_5)$).

The study also employed FTIR spectroscopy to further validate the incorporation of SeNPs into the hydrated MTA HP. The analysis revealed the presence of vibrational bands related to [$Ca(OH)_2$] at 3665 cm^{-1}, indicating the continued presence of this compound. However, the band related to adsorbed water, observed in the hydrated MTA HP before the incorporation of SeNPs, disappeared at 3440 cm^{-1}.

The study also identified other bands, including (CO_3) groups related to ($CaCO_3$) formation at 713, 1413, and 1470 cm^{-1}. Additionally, the presence of (Si–O) bands at 798 and 516 cm^{-1} was detected, along with a peak at 418 cm^{-1} attributed to the lattice vibration (Ca–O) of hydrated tricalcium aluminate. These findings demonstrate the successful incorporation of green-synthesized SeNPs into hydrated MTA HP, resulting in structural and chemical modifications. The improved properties of this material open up a range of potential applications, including advanced repair and regeneration of dental and bone tissues. The implications of this research are substantial as it paves the way for further advancements in the field of biomaterials and tissue engineering. By harnessing the unique properties of green-synthesized SeNPs, we can potentially develop more effective and biocompatible materials for various medical applications.

Table 4 presents the infrared spectral analysis of the functional group bands in the hydrated MTA after the addition of SeNPs. These findings offer valuable insights into the chemical modifications and interactions within the material, highlighting the impact of the nanoparticle incorporation.

The analysis of the infrared spectrum reveals several important findings. The bands related to (CSH) experience shifts, indicating interaction with the SeNPs. Moreover, new bands associated with calcium selenite,

Table 4: Infrared spectral analysis of functional group bands in hydrated MTA after incorporation of selenium nanoparticles

Band position (cm^{-1})	Functional group	Observation
1650	CSH	Shifted[15]
1778 and 1695	Calcium selenite (Se=O)	Newly appeared[22]
1100, 1152, and 495	CSH	Shifted[30]
1082 and 440	(Se–O) bending vibration group	Newly appeared[23,24]
837	Selenite (SeO_3)	Weak band observed[25]
3665	Ca $(OH)_2$	Present[15]
3440	Adsorbed water	Disappeared
2950	CH_2 stretching (PVP)	Present[20]
713, 1413, and 1470	(CO_3) group ($CaCO_3$)	Present[9]
798 and 516	Si–O	Present[9]
418	(Ca–O) lattice vibration (hydrated tricalcium aluminate)	Observed

MTA = mineral trioxide aggregate, PVP = Polyvinylpyrrolidone, CSH = calcium silicate hydrate

characterized by (SeO_3^{-2}) and (Se=O) stretching vibrations, emerge after the incorporation of SeNPs. The disappearance of the adsorbed water band and the presence of characteristic bands related to [$Ca(OH)_2$] confirm the integrity of the hydrated MTA in the material. The identification of (Si–O) bands suggests the involvement of silica, which confirms the interaction between the SeNPs and the material's structure. Finally, this spectral analysis provides a comprehensive understanding of the changes and interactions within the hydrated MTA after incorporating SeNPs. These findings contribute to the knowledge of the material's enhanced properties and its potential applications in various fields, particularly in dental and bone tissue repair.

X-RAY DIFFRACTION

Table 5 presents the 2θ values of the characteristic peaks observed in the hydrated MTA Repair HP (after setting) materials. These peaks correspond to specific crystal phases, providing valuable information about the material's composition and structural properties.

The table summarizes the 2θ values corresponding to the characteristic peaks observed in the hydrated MTA Repair HP (after setting) materials. These values are indicative of the presence of specific crystal phases within the material. The XRD pattern, depicted in Figure 3, of the experimental MTA Repair HP (after setting) showed peaks corresponding to portlandite [$Ca(OH)_2$], is a reactional byproduct, and ($CaCO_3$) was observed. Furthermore, the characteristic peaks corresponding to ($Ca_3Al_2O_6$) were absent after the hydration and setting reactions, as documented in Table 4. This signifies the transformation and alteration of the material's crystalline structure. Upon hydration of MTA Repair HP, we identified the peaks at 2θ = 18.00°, 28.67°, 34.10°, 47.12°, and 54.35° as indicative of the formation of [$Ca(OH)_2$] [PDF 00-044-1481]. Interestingly, these peaks merged with the peaks of ($CaWO_4$) at 2θ = 18.62°, 28.72°, 34.17°, 47.11°, and 54.31° observed in the same positions. Moreover, additional ($CaWO_4$) peaks were detected at 31.43°, 39.19°, 43.32°, 49.10°, 56.30°, 57.88°, 59.48°, and 76.10°.

Table 5: Characteristic peak 2θ values of hydrated MTA Repair HP (after setting)

Crystal phase	2θ of characteristic peaks (°)
Ca_3SiO_5	32.19°, 39.55°, 45.69°, 47.01°, 49.07°, and 56.38°
Ca_2SiO_4	31.75°, 32.14°, 32.57°, 34.31°, 39.43°, 45.56°, and 57.90°
$CaWO_4$	18.62°, 28.72°, 31.43°, 34.17°, 39.19°, 43.32°, 47.11°, 49.10°, 54.31°, 56.30°, 57.88°, 59.48°, and 76.10°
$Ca(OH)_2$	18.00°, 28.67°, 34.10°, 47.12°, and 54.35°
$Ca_2Al_2O_5{\cdot}8H_2O$	31.13°, 39.13°, 43.09°, 49.33°, and 57.71°
$CaCO_3$	31.51°, 39.48°, 43.24°, 47.21°, 56.67°, 57.51°, and 76.43°

MTAHP = mineral trioxide aggregate high plasticity

Furthermore, we identified peaks at 2θ = 31.13°, 39.13°, 43.09°, 49.33°, and 57.71° that matched with the characteristic peaks of Calcium Aluminum Oxide Hydrate ($Ca_2Al_2O_5{\cdot}8H_2O$) [PDF 00-045-0564]. This finding provides additional evidence of structural transformations in the hydrated MTA Repair HP material. The phase identification was conducted using search-match software, utilizing the JCPDS-ICDD files. This rigorous analysis confirms the changes and reactions occurring in the hydrated MTA Repair HP material. These findings significantly contribute to our understanding of the structural modifications and reactions that take place during the hydration and setting of MTA Repair HP.

Characterization of green-synthesized SeNPs has also been studied. Through XRD spectrum analysis, we have successfully identified the crystal structure, lattice constants, and average crystalline size of the SeNPs, providing valuable insights into their properties. The XRD spectrum analysis confirmed the presence of distinct diffraction peaks at 2θ (degrees) values of 23.51°, 29.70°, 41.30°, 43.64°, 45.35°, 48.10°, 51.72°, 55.66°, 56.14°, 61.21°, 65.23°, 68.25°, and 71.59°. These peaks correspond to the (100), (101), (110), (102), (111), (200), (201), (003), (112), (103), (210), (211), and (113) planes of the SeNPs, as shown in Figure 2. The diffraction peaks observed in the XRD spectrum are indicative of the hexagonal structure of the SeNPs. These values are in excellent agreement with the standard ICDD card no. (00-006-0362), validating the crystal structure of the synthesized SeNPs.

The 2θ values represent the diffraction angles at which significant scattering occurs, providing information about the crystal structure of the nanoparticles. The FWHM indicates the broadening of the diffraction peaks, reflecting the crystalline imperfections and size within the SeNPs powder sample. Using the Debye–Scherrer equation, the crystal size (D) was calculated based on the FWHM values for each peak. The calculated crystal sizes range from 48.61403 to 56.82401 nm, with a mean value of ≈52 nm. These

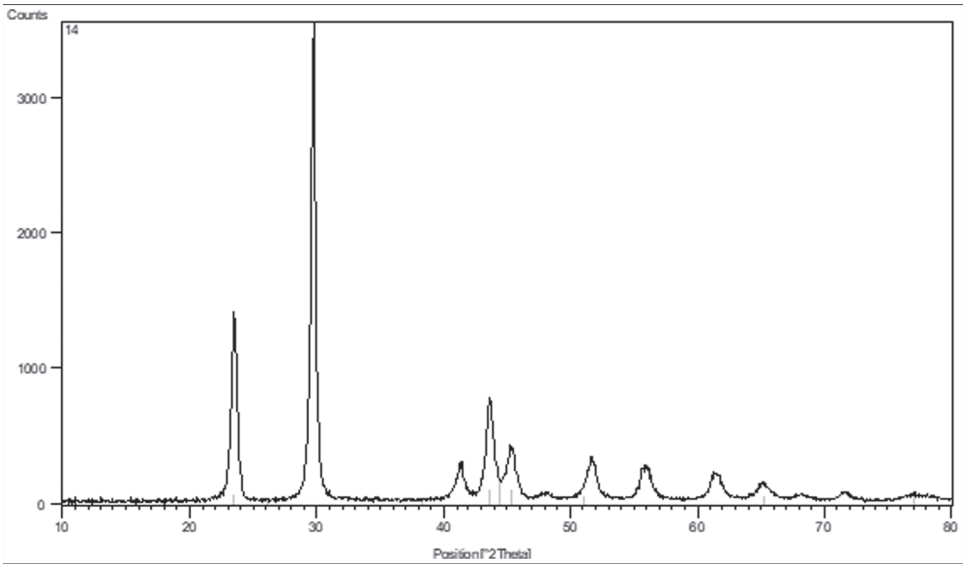

Figure 2: XRD pattern of the SeNPs. XRD = X-ray diffraction, SeNPs = selenium nanoparticles

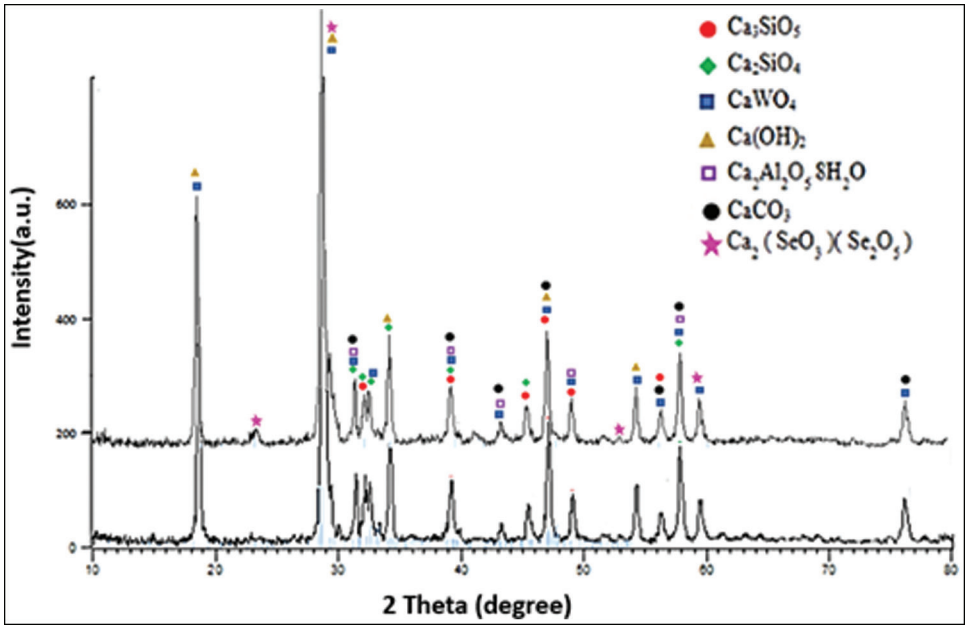

Figure 3: XRD pattern of hydrated MTA HP prior to and following incorporation of SeNPs. XRD = X-ray diffraction, MTA HP = mineral trioxide aggregate high plasticity, SeNPs = selenium nanoparticles

results provide important insights into the crystal size of the green-synthesized SeNPs. Understanding the size and crystallinity of the nanoparticles is crucial for assessing their properties and potential applications in various fields. The precise control of the crystal size and structure can greatly influence the nanoparticles' performance and functionality.

The XRD analysis results of the hydrated MTA Repair HP material incorporated with green-synthesized SeNPs after setting are also investigated. Through careful examination of the XRD pattern, as depicted in Figure 3, we have made significant observations regarding the structural changes and formation of new phases in the material. The analysis revealed the emergence of new peaks in the XRD pattern of the experimental MTA HP incorporated with SeNPs compared to the hydrated MTA HP without SeNPs. These new peaks, observed at 2θ (degrees) values of 23.62°, 29.24°, 34.07°, 39.39°, 53.46°, and 59.51°, correspond to the formation of calcium selenite. This observation is supported by the reference code (PDF 00-048-0370). Furthermore, the peaks corresponding to $Ca_3Al_2O_6$ were no longer present after the hydration

Table 6: Characteristic peak 2θ values of experimental hydrated MTA Repair HP incorporated with SeNPs (after setting)

Crystal phase	2θ of characteristic peaks (°)
Ca_3SiO_5	32.19°, 39.55°, 45.69°, 47.01°, 49.07°, and 56.38°
Ca_2SiO_4	31.75°, 32.14°, 32.57°, 34.31°, 39.43°, 45.56°, and 57.90°
$CaWO_4$	18.62°, 28.72°, 31.43°, 34.17°, 39.19°, 43.32°, 47.11°, 49.10°, 54.31°, 56.30°, 57.88°, 59.48°, and 76.10°
$Ca(OH)_2$	18.00°, 28.67°, 34.10°, 47.12°, and 54.35°
$Ca_2Al_2O_5{\cdot}8H_2O$	31.13°, 39.13°, 43.09°, 49.33°, and 57.71°
$CaCO_3$	31.51°, 39.48°, 43.24°, 47.21°, 56.67°, 57.51°, and 76.43°
$Ca_2(SeO_3)(Se_2O_5)$	23.62°, 29.24°, 34.07°, 39.39°, 53.46°, and 59.51°

MTAHP = mineral trioxide aggregate high plasticity, SeNPs = Selenium nanoparticles

and setting reactions, suggesting their transformation or disappearance. Instead, new peaks associated with calcium aluminum oxide hydrate, [$Ca(OH)_2$], and $CaCO_3$ structures were observed, characterized by their characteristic peak angles.

Table 6 provides the 2θ values of the characteristic peaks observed in the XRD spectrum of the experimental MTA HP incorporated with SeNPs after setting. These values offer detailed information about the crystallographic orientation and identification of the phases present in the material.

The characteristic peaks of Ca_3SiO_5, Ca_2SiO_4, $CaWO_4$, $Ca(OH)_2$, $Ca_2Al_2O_5{\cdot}8H_2O$, and $CaCO_3$ have been previously identified in the hydrated MTA Repair HP material. The addition of SeNPs introduces new peaks corresponding to the $Ca_2(SeO_3)(Se_2O_5)$ phase, observed at 2θ values of 23.62°, 29.24°, 34.07°, 39.39°, 53.46°, and 59.51°. These characteristic peaks provide insights into the structural modifications and the formation of the main phases in the experimental hydrated MTA Repair HP material after the incorporation of SeNPs. The XRD analysis, coupled with the characterization of the hydrated MTA Repair HP incorporated with SeNPs, contributes to the advancement of our knowledge regarding these materials. The XRD analysis results provide valuable insights into the structural modifications and formation of new phases in the hydrated MTA Repair HP material after the incorporation of SeNPs. The observed changes have implications for the material's properties and potential applications in various fields, including dentistry and bone tissue repair.

Discussion

Setting time

The MTA is a calcium silicate-based hydraulic cement used in various endodontic applications. It consists mainly of calcium silicate compounds, such as Ca_3SiO_5 and Ca_2SiO_4, along with trace amounts of radiopacifier. The setting process of MTA involves the hydration of its key components, namely tricalcium silicate (C_3S), dicalcium silicate (C_2S), and tricalcium aluminate. These reactions lead to the formation of amorphous CSH gels, [$Ca(OH)_2$] crystals, and calcium aluminum oxide hydrate crystals. The intermingling and consolidation of these components contribute to the self-setting[8] properties of MTA.

In this study, the initial setting time of MTA HP was found to be 15 min, indicating a rapid initial setting rate. This aligns with previous research[9] that confirmed the quick initial setting of MTA Repair HP dental material. The early setting is primarily attributed to the hydration of the calcium silicates, which produce CSH gels and [$Ca(OH)_2$] crystals.[10] The high surface area of the MTA HP material, resulting from small particle sizes,[11,12] may also contribute to its quick setting time.[10] However, the final setting time of MTA Repair HP was observed to be 85 min, by the manufacturer's instructions. The addition of plasticizer in the liquid formulation of the cement and the absence of compositional sulfate phases, along with its high aluminum content, contribute to the shorter final setting time.[12] The results of the study also demonstrated a further decrease in the setting time of MTA HP with the incorporation of different concentrations of SeNPs. This can be attributed to the reduction in particle size, which increases surface area and reactivity of the cement components.[12] The addition of SeNPs leads to the formation of calcium selenite, which contributes to the heat-emitting reaction and accelerates the setting speed. The disappearance of the water band in the ATR-FTIR analysis further supports the role of SeNPs in shortening the setting time. In summary, the incorporation of SeNPs in MTA HP results in a linear decrease in the setting time, attributed to the heat-emitting reaction,[10] increased surface area, higher reactivity,[13,14] and the formation of calcium selenite. These findings highlight the potential for SeNPs to accelerate the setting time of MTA HP and improve its properties as a dental material.

Fourier transform infrared spectroscopy with attenuated total reflectance

The ATR-FTIR data spectra pattern of the MTA (after setting) in this study confirmed the main reactional

byproducts observed were CSH and [$Ca(OH)_2$], along with $CaCO_3$, C_3S, and C_2S, as indicated by their functional groups' bands spectra. These findings are consistent with a study by Jiménez-Sánchez *et al*.[9] The chemical reactions involve the hydration of calcium silicate compounds, resulting in the production of a CSH gel, which is responsible for setting and the formation of [$Ca(OH)_2$]. The ATR-FTIR data revealed specific bands related to the vibrations of (O–H) adsorbed water molecules and (O–H) from [$Ca(OH)_2$]. Similar observations were made by Jiménez-Sánchez *et al*.[9] Furthermore, Pedrosa *et al*.[15] demonstrated that the band at 3640 cm^{-1} originates from the (O–H) stretching mode of the hydration product [$Ca(OH)_2$]. These results provide confirmation and a good link with the XRD results, which indicated the presence of [$Ca(OH)_2$] in the set forms of the tested materials. The ATR-FTIR results also showed the formation of CSH through their functional groups at specific wavenumbers. The presence of bands at 495, 656, 925, 1100, 1152, and 1650 cm^{-1} indicated CSH formation, which is important for tracking amorphous phases, particularly CSH gel. Another significant observation was the appearance of a band at ~1010 cm^{-1}, attributed to the main hydration product (CSH), in the silicate region of the spectrum. This band appears when the intensities of the bands assignable to water and C_3S start to decrease.[9]

Also, the (O–H) stretching vibrational band for [$Ca(OH)_2$] was observed at 3644 cm^{-1}.[15] Wavenumbers at 925, 1100, and 1152 cm^{-1} indicate calcium silicate unit dissolution to form CSH.[9,16,17] The Si–O–Si bending vibrations of CSH were detected in this study at 656 cm^{-1},[18] the appearance of (Al–O) band at 860 cm^{-1} was explained that the Al as a hydration active element and the lattice vibration (Ca–O) of hydrated tricalcium aluminate was observed at 422 cm^{-1}.[9,19] The hydrated MTA HP exhibited a band at 2950 cm^{-1}, indicating CH_2 stretching of polyvinylpyrrolidone.[20] The presence of carbonate groups (CO_3^{2-}) was confirmed by bands at 1470 and 1413 cm^{-1}, resulting from reactions of atmospheric (CO_2) with [$Ca(OH)_2$].[9] These findings were consistent with other studies that also observed carbonate group formation. After hydration, vibrational bands corresponding to (Si–O) stretching at 798 cm^{-1} characteristic of (Ca_3SiO_5) were observed in this study.[21] The bending group (SiO_4) in this study was detected at 517 cm^{-1}, due to calcium silicate anhydrate (SiO_4^{2-}) of C_3S while the (SiO_4) bending group at 450 cm^{-1} indicated (Ca_2SiO_4).[15]

The results of the ATR-FTIR spectrum of the hydrated MTA HP incorporated with green-synthesized SeNPs revealed the presence of new bands corresponding to calcium selenite. These bands were observed at 1778 and 1659 cm^{-1}, indicating stretching vibrations of the (Se=O) and (SeO_3^{-2}) groups.[22] The appearance of these bands may be attributed to the shifting of the CSH band at 1650 cm^{-1}. Additionally, new bands at 1082 and 440 cm^{-1} were observed, which correspond to the (Se–O) bending vibration group.[23,24] These bands may be due to the shifting of the CSH band at 1100 and 1152 cm^{-1}. The (Se–O) bending vibration group at 440 cm^{-1} was also detected, possibly resulting from the shifting of the CSH band at 495 cm^{-1}. Moreover, a weak band at 837 cm^{-1} was attributed to the stretching vibration of the selenite (SeO_3) group,[25] indicating the reaction between CSH and SeNPs. This band may be the result of the shifting of the CSH band at 656 cm^{-1}. These findings confirm the interaction between CSH and SeNPs, suggesting the replacement of selenium with silica within the CSH structure, resulting in the formation of calcium selenite.

These findings demonstrate the successful incorporation of green-synthesized SeNPs into the hydrated MTA HP, resulting in the formation of calcium selenite. This novel material shows promising potential for various applications, benefiting from the unique properties of SeNPs in combination with MTA's advantageous properties.

X-ray diffraction

The XRD analysis of the hydrated MTA HP material before the incorporation of SeNPs revealed important findings. When the supplied liquid molecules came in contact with the MTA HP powder, the analysis showed the presence of phases, such as (Ca_3SiO_5) and (Ca_2SiO_4), indicating the composition of calcium silicates in the material. The result of this study showed similar observations made by Choi *et al*.,[10] who reported peaks assigned to the $Ca_3Al_2O_6{\cdot}6H_2O$ phase appeared after setting. The result of this study also as many studies that identified the main chemical composition of MTA Repair HP as calcium silicates in the form of (Ca_3SiO_5), (Ca_2SiO_4), and ($Ca_3Al_2O_6$), along with calcium tungstate ($CaWO_4$) as a radiopacifier element.[9] The XRD result confirmed the occurrence of chemical reactions among the components of the powder and liquid, leading to setting. The formation of CSH and [$Ca(OH)_2$] was supported by the appearance of peaks at 2θ = 18.00°, 28.67°, 34.10°, 47.12°, and 54.35°, which are used to identify the production of [$Ca(OH)_2$]. However, the identification of CSH peaks through XRD analysis was challenging due to the poorly crystallized nature of CSH and its nanoscale crystalline structure, which appears amorphous in XRD analysis.[26]

Moreover, the XRD results indicated the appearance of peaks at 31.13°, 39.13°, 43.09°, 49.33°, and 57.71°, matching with the ($Ca_2Al_2O_5{\cdot}8H_2O$) phase, suggesting

the involvement of aluminum in the hydration process.[9] Additionally, new peaks at 2θ of 31.51°, 39.48°, 43.24°, 47.21°, 56.67°, 57.51°, and 76.43° were associated with ($CaCO_3$), resulting from the reaction of [$Ca(OH)_2$] with atmospheric CO_2 after hydration.[26]

The XRD analysis for SeNPs provided important insights into their crystal structure and purity. The observed peaks in the XRD profile figure were found to be in good agreement with the standard ICDD data for SeNPs, specifically corresponding to a hexagonal crystal structure. This hexagonal structure has been reported in other studies as well.[27] In Figure 2, the XRD analysis of the green-synthesized SeNPs exhibited clear and sharp Bragg reflections. The Bragg reflection peaks observed at various 2θ angles, such as 23.51°, 29.70°, 41.30°, 43.64°, and others, were attributed to the (100), (101), (110), (102), (111), (200), (201), (003), (112), (103), (210), (211), and (113) reflections of the pure hexagonal phase of Se crystal. The sharpness of these peaks indicates a high degree of crystallinity of the green-synthesized SeNPs. The absence of diffraction peaks related to impurities further confirms the purity of the SeNPs.[28] The mean crystallite size of the SeNPs was determined to be 52.10 nm using Debye–Scherrer's formula.

The XRD analysis of the hydrated MTA Repair HP material after incorporating green-synthesized SeNPs revealed important changes compared to MTA HP without SeNPs. Upon analysis, a new peak at 2θ of 23.62° was observed, indicating the formation of crystalline calcium selenite. This peak can be attributed to the presence of calcium selenite, as confirmed by the reference code (PDF 00-048-0370) that represents the characteristic fingerprint of this compound in XRD analysis. Furthermore, additional peaks corresponding to calcium selenite were registered at 2θ angles of 29.24°, 34.07°, 39.39°, 53.46°, and 59.51°. These peaks further support the presence of crystalline calcium selenite in the hydrated MTA Repair HP material after incorporating SeNPs. Moreover, the XRD analysis revealed a decrease in the intensity of peaks corresponding to (Ca_3SiO_5) and (Ca_2SiO_4). This decrease in intensity may be attributed to the acceleration of the setting reaction in the presence of SeNPs. The incorporation of SeNPs appears to affect the setting kinetics of the MTA Repair HP, leading to changes in the crystalline phases present in the material. These findings highlight the successful incorporation of green-synthesized SeNPs into the MTA The repair of HP material leads to the development of crystalline calcium selenite, which could prove advantageous as it can serve as a substitute for calcium phosphate—a vital component in the healing process.[29] The observed changes in XRD peaks and intensities indicate the interaction between SeNPs and the MTA matrix, potentially influencing the material's properties and behavior. The study's hypothesis was disproven, as the results revealed an influence of SeNPs on the setting time of MTA HP, accompanied by the observed chemical reaction through FTIR analysis depending on the concentration of SeNPs that was added.

Conclusions

In conclusion, the addition of SeNPs to MTA HP has a different effect on the setting time of MTA HP pulp capping material depending on the concentration of SeNPs powder. The research conducted thus far has yielded promising results. The incorporation of 0.5% w/w SeNPs had no significant effect on the initial setting time, making it suitable for practical implementation. However, other concentrations did lead to a decrease in the initial setting time. Notably, the 1% w/w concentration group showed a significant difference compared to the other groups. Various concentrations of SeNPs also resulted in a shorter final setting time, indicating improved efficiency during dental procedures. The 1% w/w and 1.5% w/w concentration groups did not exhibit a significant difference in the final setting time. The successful repair of HP material culminates in the formation of crystalline calcium selenite, presenting a promising outcome. This remarkable development holds significant potential as it could serve as a viable alternative to calcium phosphate, a crucial element in the healing process. The utilization of crystalline calcium selenite opens new possibilities for advancing medical treatments and enhancing overall healing capabilities, heralding a bright future in the field of regenerative medicine.

Authors contributions

Njwan Fadhel Shehab: Conceptualization, design, data acquisition, analysis, statistical analysis, manuscript preparation, editing, and review. Nadia Hameed Hasan: Conceptualization, design, intellectual content definition, literature search, data analysis, manuscript preparation, editing, and review. Hana Khaleel Ismail: Conceptualization, design, intellectual content definition, manuscript preparation, editing, and review.

Acknowledgements

The authors express their gratitude to the University of Mosul, specifically the College of Dentistry, for their valuable contributions and support throughout this work.

Financial support and sponsorship

None provided..

Conflicts of interest

No conflicts of interest exist.

Ethical policy and institutional review board statement

Not available

Patient declaration of consent

Not available

Data availability statement

All data generated or analyzed in this study are included in the paper.

References

1. Hadrup N, Loeschner K, Skov K, Ravn-Haren G, Larsen EH, Mortensen A, *et al*. Effects of 14-day oral low dose selenium nanoparticles and selenite in rat—As determined by metabolite pattern determination. PeerJ 2016;4:e2601.
2. Shahmoradi S, Shariati A, Amini SM, Zargar N, Yadegari Z, Darban-Sarokhalil D. The application of selenium nanoparticles for enhancing the efficacy of photodynamic inactivation of planktonic communities and the biofilm of Streptococcus mutans. BMC Res Notes 2022;15:84.
3. Doğan MS. Relation of trace elements on dental health. In: Trace Elements-Human Health and Environment, Ch. 4. 2018; 5:71-83.
4. Hou J, Tamura Y, Lu H-Y, Takahashi Y, Kasugai S, Nakata H, *et al*. An in vitro evaluation of selenium nanoparticles on osteoblastic differentiation and antimicrobial properties against *Porphyromonas gingivalis*. Nanomaterials (Basel) 2022;12:1850.
5. Hossain N, Islam MA, Chowdhury MA, Alam A. Advances of nanoparticles employment in dental implant applications. Appl Surf Sci Adv 2022;12:100341.
6. Mahmoud O, Al-Afifi NA, Salihu Farook M, Ibrahim MA, Al Shehadat S, Alsaegh MA. Morphological and chemical analysis of different types of calcium silicate-based cements. Int J Dent 2022;2022:1-16.
7. Venkatesan A, Sujatha V. Green synthesis of selenium nanoparticle using leaves extract of *Withania somnifera* and its biological applications and photocatalytic activities. BioNanoScience 2019;9:105-16.
8. Liu W, Chang J, Yue Z. Physicochemical properties and biocompatibility of tricalcium and dicalcium silicate composite cements after hydration. Int J Appl Ceram Technol 2011;8:560-5.
9. Jiménez-Sánchez MC, Segura-Egea JJ, Díaz-Cuenca A. Higher hydration performance and bioactive response of the new endodontic bioactive cement MTA HP Repair compared with ProRoot MTA white and NeoMTA plus. J Biomed Mater Res B Appl Biomater 2019;107:2109-20.
10. Choi HW, Um SH, Rhee SH. Synthesis of a Ca_3SiO_5–Ca_2SiO_4–$Ca_3Al_2O_6$ cement system with rapid setting capacity by spray-pyrolysis coupled with sol–gel method. J Biomed Mater Res B Appl Biomater 2019;107:1440-51.
11. Ha WN, Bentz DP, Kahler B, Walsh LJ. D90: The strongest contributor to setting time in mineral trioxide aggregate and Portland cement. J Endod 2015;41:1146-50.
12. Galarça AD, Da Rosa WLO, Da Silva TM, da Silveira Lima G, Carreño NLV, Pereira TM, *et al*. Physical and biological properties of a high-plasticity tricalcium silicate cement. Biomed Res Int 2018;2018:8063262.
13. Buzea C, Pacheco II, Robbie K. Nanomaterials and nanoparticles: Sources and toxicity. Biointerphases 2007;2:MR17-71.
14. Joudeh N, Linke D. Nanoparticle classification, physicochemical properties, characterization, and applications: A comprehensive review for biologists. J Nanobiotechnol 2022;20:262.
15. Pedrosa MS, Vilela HS, Rahhal JG, Bueno NP, Lima FS, Nogueira FN, *et al*. Exposure to lipopolysaccharide and calcium silicate-based materials affects the behavior of dental pulp cells. Braz Dent J 2022;33:9-17.
16. Ylmén R, Jäglid U, Steenari B-M, Panas I. Early hydration and setting of Portland cement monitored by IR, SEM and Vicat techniques. Cement Concrete Res 2009;39:433-9.
17. del Carmen Jiménez-Sánchez M, Segura-Egea JJ, Díaz-Cuenca A. MTA HP Repair stimulates in vitro an homogeneous calcium phosphate phase coating deposition. J Clin Exp Dent 2019;11:e322.
18. Madadi A, Wei J. Characterization of calcium silicate hydrate gels with different calcium to silica ratios and polymer modifications. Gels 2022;8:75.
19. Taddei P, Modena E, Tinti A, Siboni F, Prati C, Gandolfi MG. Effect of the fluoride content on the bioactivity of calcium silicate-based endodontic cements. Ceram Int 2014;40:4095-107.
20. Rahma A, Munir MM, Prasetyo A, Suendo V, Rachmawati H. Intermolecular interactions and the release pattern of electrospun curcumin-polyvinyl (pyrrolidone) fiber. Biol Pharm Bull 2016;39:163-73.
21. Del Bosque IS, Martínez-Ramírez S, Blanco-Varela MT. FTIR study of the effect of temperature and nanosilica on the nano structure of C–S–H gel formed by hydrating tricalcium silicate. Constr Build Mater 2014;52:314-23.
22. Daoud KM, Saleh MY. Synthesis and antibacterial evaluation of some 1, 2, 3-selenadiazole derivatives. J Educ Sci 2013;26:14-22.
23. Kurze R, Peatzold R. Untersuchungen an Selen-Verbindungen LVIII Uber die Addukte des Selentrioxids mit Trimethylamin und Pyridin. Zeitschrift für anorganische und allgemeine Chemie 1972;387:367-72.
24. Micka Z, Uchytilova M, Ebert M. Cadmium(II) and mercury(II) selenites. Chem Papers 1984;38:759-70.
25. Alkan B, Durucan C. Complete chemical and structural characterization of selenium-incorporated hydroxyapatite. J Mater Sci Mater Med 2022;33:5.
26. Lee Y-L, Wang W-H, Lin F-H, Lin C-P. Hydration behaviors of calcium silicate-based biomaterials. J Formos Med Assoc 2017;116:424-31.
27. Qureshi F, Nawaz M, Ansari MA, Khan FA, Berekaa MM, Abubshait SA, *et al*. Synthesis of M-Ag_3PO_4,(M= Se, Ag, Ta) nanoparticles and their antibacterial and cytotoxicity study. Int J Mol Sci 2022;23:11403.
28. Mulla NA, Otari SV, Bohara RA, Yadav HM, Pawar SH. Rapid and size-controlled biosynthesis of cytocompatible selenium nanoparticles by *Azadirachta indica* leaves extract for antibacterial activity. Mater Lett 2020;264:127353.
29. Ressler A, Antunović M, Cvetnić M, Ivanković M, Ivanković H. Selenite substituted calcium phosphates: Preparation, characterization, and cytotoxic activity. Materials 2021;14:3436.
30. Mollah M, Yu W, Schennach R, Cocke DL. A Fourier transform infrared spectroscopic investigation of the early hydration of Portland cement and the influence of sodium lignosulfonate. Cement Concrete Res 2000;30:267-73.
31. Okamura T, Chen L, Tsumano N, Ikeda C, Komasa S, Tominaga K, *et al*. Biocompatibility of a high-plasticity, calcium silicate-based, ready-to-use material. Materials 2020;13:4770.
32. Abu Zeid ST, Alamoudi NM, Khafagi MG, Abou Neel EA. Chemistry and bioactivity of NeoMTA Plus™ versus MTA Angelus® root repair materials. J Spectrosc 2017;2017:8736428.